

## Nonlinear Gyrokinetic Simulations of Ion-Temperature-Gradient Turbulence for the Optimized Wendelstein 7-X Stellarator

P. Xanthopoulos,<sup>1</sup> F. Merz,<sup>2</sup> T. Görler,<sup>2</sup> and F. Jenko<sup>2</sup>

<sup>1</sup>Max-Planck-Institut für Plasmaphysik, Teilinstitut Greifswald, Wendelsteinstrasse 1, D-17491 Greifswald, Germany

<sup>2</sup>Max-Planck-Institut für Plasmaphysik, Boltzmannstrasse 2, D-85748 Garching, Germany

(Received 5 April 2007; published 20 July 2007)

Ion-temperature-gradient turbulence constitutes a possibly dominant transport mechanism for optimized stellarators, in view of the effective suppression of neoclassical losses characterizing these devices. Nonlinear gyrokinetic simulation results for the Wendelstein 7-X stellarator [G. Grieger *et al.*, in *Proceedings of the IAEA Conference on Plasma Physics and Controlled Nuclear Fusion Research, 1990* (IAEA, Vienna, 1991) Vol. 3, p. 525]—assuming an adiabatic electron response—are presented. Several fundamental features are discussed, including the role of zonal flows for turbulence saturation, the resulting flux-gradient relationship, and the coexistence of ion-temperature-gradient modes with trapped ion modes in the saturated state.

DOI: 10.1103/PhysRevLett.99.035002

PACS numbers: 52.65.Tt, 52.30.Gz, 52.35.Ra, 52.55.Hc

Optimized stellarators [1] are recognized as promising candidates for the realization of a fusion power plant on the basis of magnetic confinement. A key feature of this family of devices—one representative being the Wendelstein 7-X (W7-X) stellarator which is currently under construction—is the effective suppression of neoclassical losses due to the special design of the magnetic geometry. This fact renders ion-temperature-gradient (ITG) turbulence [2] a prominent mechanism of thermal transport.

The theoretical understanding of turbulent transport is generally based on numerical solutions of the nonlinear gyrokinetic equations [3]. But while there is an abundance of publications on plasma turbulence in axisymmetric devices (tokamaks), not much is known about its character in nonaxisymmetric geometries (see, however, Refs. [4,5]). In fact, to our knowledge, the present work constitutes the first attempt to investigate turbulent transport in an optimized stellarator, using nonlinear gyrokinetics and a realistic magnetic equilibrium. As we will see, the properties of ITG turbulence in such a system are very interesting. They include strong zonal flow (ZF) activity accompanied by relatively moderate transport levels, as well as the coexistence of ITG modes with trapped ion modes in the saturated state.

Several linear microinstability analyses (see, e.g., Refs. [6,7] and various references therein) suggest that the detailed magnetic geometry of a given stellarator is likely to play an important role in determining its turbulence properties. This raises the question in which way the optimizations underlying the design of a modern stellarator like W7-X affect both neoclassical *and* anomalous transport. In this Letter, we employ a realistic three-dimensional vacuum ( $\beta = 0$ ) equilibrium (termed hs5v10u [8]) to address this important issue.

The main tool for our numerical investigation is the massively parallel gyrokinetic turbulence code GENE [9,10] which has been upgraded recently to also tackle

nonaxisymmetric geometries in the framework of a flux-tube approach [11]. The necessary field line tracing starts from the outboard midplane in the “bean-shaped” plane at a radial distance of  $R_0 = 6.0$  m from the central axis (see Fig. 1). Since the safety factor is  $q \approx 6/5$  and the device has a fivefold discrete symmetry, all geometric coefficients are periodic after one poloidal turn, and it is sufficient to track the field line (only) that far. Moreover, due to a global magnetic shear of  $\hat{s} \approx 0$ , the boundary conditions in all three spatial directions may be taken to be periodic. A detailed description of the geometry, the form of the equations, and the normalization convention is available in Ref. [11].

The present analysis is restricted to adiabatic (Boltzmann) electrons, allowing for longer and better resolved runs—simulations with nonadiabatic electrons are left for future work. In terms of our baseline physical parameters, we choose  $R/L_{T_i} = 18$  and  $R/L_n = 0$  (here,  $R = R_0$ ) for the normalized radial ion temperature and

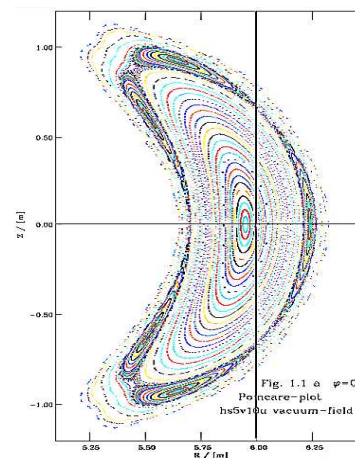


FIG. 1 (color online). Starting point of the traced flux tube on the bean-shaped plane of the W7-X stellarator.

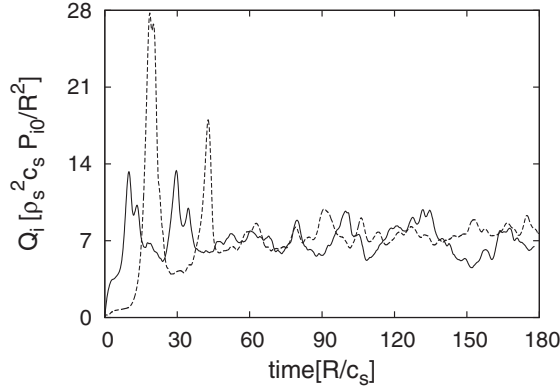


FIG. 2. Time history of the turbulent ion heat flux for our baseline parameters and nominal (solid line) or increased (dashed line) wave number space resolution, showing convergence.

density gradients, respectively, and  $T_e/T_i = 1$ . The computations are performed on a spatial domain of  $(L_x, L_y) = (64\rho_s, 64\rho_s)$  [or  $(128\rho_s, 128\rho_s)$ ], where  $\rho_s = c_s/\Omega_i$  (here,  $c_s = \sqrt{T_{e0}/m_i}$  is the ion sound speed and  $\Omega_i$  the ion Larmor frequency). For the discretization,  $N_x \times N_y \times N_z = 48 \times 32 \times 96$  [or  $128 \times 64 \times 100$ ] grid points are employed in the radial, diamagnetic, and parallel directions, respectively, whereas in velocity space,  $N_{v_{\parallel}} \times N_{\mu} = 32 \times 8$  grid points are used. The adequacy of this phase space resolution for the present simulations has been confirmed by means of linear runs (changing  $N_z$ ,  $N_{v_{\parallel}}$ , and  $N_{\mu}$ ) [7] and the nonlinear runs shown in Fig. 2. Here, the time-averaged ion heat flux in the saturated phase is observed to agree quite well for the two setups described above.

As a first attempt to quantitatively characterize the transport caused by the ITG dynamics for the W7-X stellarator, we study the dependence of the ion thermal diffusivity  $\chi_i$  on the normalized ion temperature gradient  $R/L_{T_i}$ . The result of this effort is presented in Fig. 3, and three of its features are noteworthy. First, we observe a nonlinear upshift of the effective critical gradient with respect to the linear one (which has been determined in Ref. [7]) by about

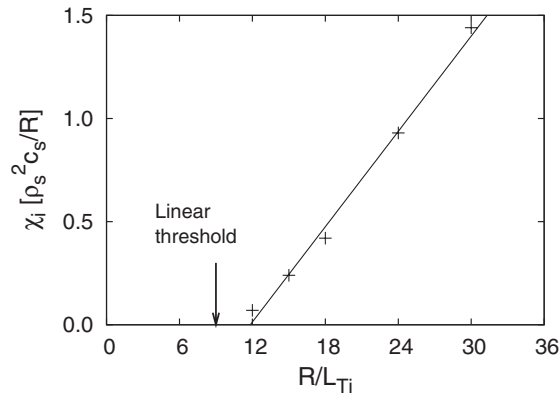


FIG. 3. Dependence of the time-averaged ion thermal diffusivity  $\chi_i$  on  $R/L_{T_i}$  for the W7-X stellarator:  $\chi_i[R/L_{T_i}]$  rises linearly and rather slowly, and there exists a Dimits shift regime.

25%. This ‘‘Dimits shift’’ [12] is known to be a characteristic property of ITG turbulence in axisymmetric geometries. Here, it is demonstrated that it is also present in the optimized stellarator W7-X. Second, the ion thermal diffusivity can be written as  $\chi_i \approx C(R/L_{T_i} - \kappa_c)(\rho_s^2 c_s/R)$  with  $C \approx 0.08$  and  $\kappa_c \approx 12$ . This means that  $\chi_i$  exhibits an offset-linear dependence on  $R/L_{T_i}$ , not the ion heat flux  $Q_i \propto (R/L_{T_i})\chi_i$  like in a tokamak (see, e.g., Ref. [12]). Third, the ‘‘stiffness factor’’  $C$  is quite small in the present case. Consequently, one obtains significant ion heat fluxes only for  $R/L_{T_i} \gg \kappa_c$ . This is in contrast to tokamaks where one usually finds much larger stiffness factors [12], implying that  $R/L_{T_i}$  will not exceed  $\kappa_c$  much for realistic  $Q_i$  values. Thus, there are significant differences between the optimized W7-X stellarator and a typical tokamak concerning the flux-gradient relationship  $Q_i[R/L_{T_i}]$ .

Other characteristics distinguishing the W7-X stellarator from the usual tokamak scenarios will be described next, using simulation data for the baseline parameters described above. In Fig. 4, we display the  $k_y$  spectrum of the time-averaged ion heat flux. One finds a double-peaked structure which is not due to bad statistics but has an interesting physical origin. The peaks at  $k_y \rho_s \approx 0.2$  and  $k_y \rho_s \approx 0.1$  are caused, respectively, by ITG modes and trapped ion modes. This can be shown, e.g., by comparing the nonlinear transport spectrum to the linear growth rate spectrum (see Fig. 5) which also has two peaks (we note in passing that the ITG branch is subject to a spectral downshift with respect to the linear spectrum which is well known from past tokamak studies; also, it is possible to move the flat spot in the spectrum shown in Fig. 4 in line with the linear expectations by changing  $R/L_{T_i}$ ). Moreover, the cross phases between various pairs of quantities are found to resemble the linear ones in the long-wavelength regime, both exhibiting a mode transition at  $k_y \rho_s \approx 0.15$ . This implies that one actually has a coexistence of these two microinstabilities also in the saturated turbulent state, a feature which raises many questions—in particular with

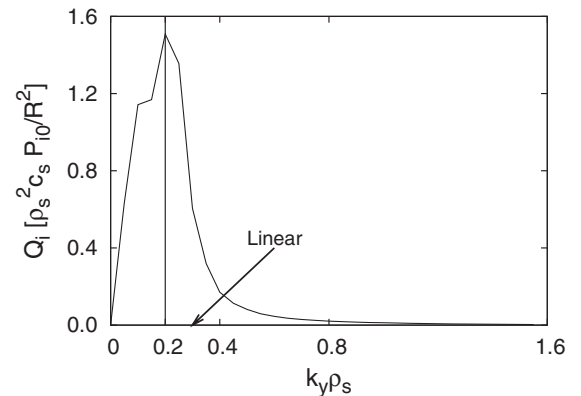


FIG. 4.  $k_y$  spectrum of the ion heat flux, exhibiting the coexistence of ITG modes (at  $k_y \rho_s \sim 0.2$ ) and trapped ion modes (at  $k_y \rho_s \sim 0.1$ ) in the saturated turbulent state.

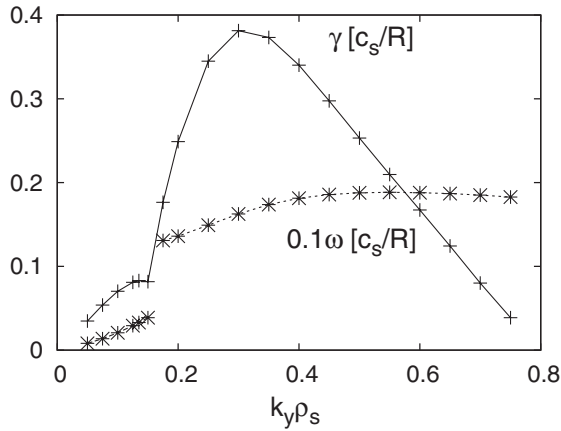


FIG. 5.  $k_y$  spectrum of the linear frequency and growth rate. The dominant microinstabilities are ITG modes (at  $k_y \rho_s > 0.15$ ) and trapped ion modes (at  $k_y \rho_s < 0.15$ ).

respect to nonlinear saturation and intermode couplings—and will be studied in more detail in future work. Another striking difference between the W7-X stellarator and a typical tokamak can be seen in the parallel mode structure of the electrostatic potential which is shown in Fig. 6. It resembles the mode structure of the underlying linear ITG mode (see Fig. 6 in Ref. [7]) and tends to peak at the positions where the bad curvature is most pronounced (see Fig. 3 in Ref. [7]), i.e., at the ends of the flux tube—corresponding to the outboard side of the device. Obviously, this nonlinear mode structure is much more complex than in the axisymmetric (“ballooning”) case, and there exists a strong zonal flow component whose role has been assessed in more detail.

Zonal flows, i.e., purely radial ( $k_y = k_{||} = 0$ ) fluctuations of the electrostatic potential, are generated nonlinearly and have the tendency to decorrelate the turbulent eddies that drive them [13]. In the present case, the measured (root mean square of the)  $\mathbf{E} \times \mathbf{B}$  shearing rate  $\omega_E$  exceeds the maximum linear growth rate  $\gamma_{\max}$  by a factor of about 10. Taking into account finite frequency correc-

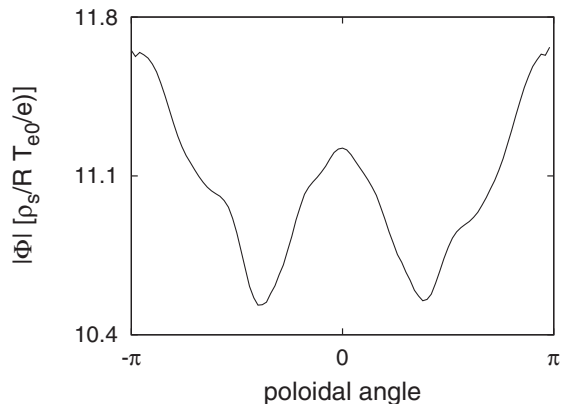


FIG. 6. Parallel mode structure of the potential fluctuations, exhibiting a rather complex behavior and a strong zonal flow component.

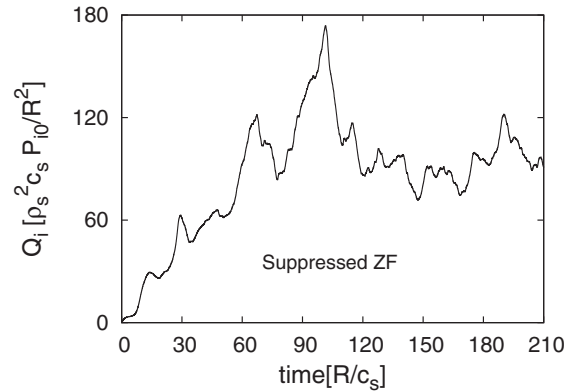


FIG. 7. Time trace of the ion heat flux for  $R/L_{T_i} = 18$  with zeroed out zonal components. The transport level is about 10 times larger than in the case with zonal flows (see Fig. 2).

tions as described in Ref. [14], one still obtains  $\omega_E \sim \gamma_{\max}$ . This suggests a significant effect of ZFs on the regulation of the turbulent transport. Next, in Fig. 7, we display the result of an ITG simulation for our baseline parameters, but with ZFs artificially suppressed. Compared with the result shown in Fig. 2, the transport level is significantly larger, and the time trace of the ion heat flux is much more intermittent. This clearly confirms that ZFs are the key nonlinear saturation mechanism under normal circumstances. However, even in the absence of zonal flows, the turbulence *does* saturate—and the transport level still remains moderate:  $\chi_i \sim 0.25 \rho_s^2 c_s / L_{T_i}$  (about one-third of the cyclone base case result for a simple tokamak geometry [12]) for  $R/L_{T_i} \sim 1.5 \kappa_c$ . For illustration, snapshots of the electrostatic potential for simulations with and without zonal flows are shown in Fig. 8. While the first case is dominated by zonal structures, suppression of ZFs leads to the appearance of distorted streamerlike structures. As pointed out before, the turbulence still saturates, a fact that raises the question of which nonlinear saturation mechanism is at work in the second case.

A scenario which has been proposed in Refs. [15,16] is based on the notion of secondary instabilities. The latter are driven by gradients in the primary mode structure and

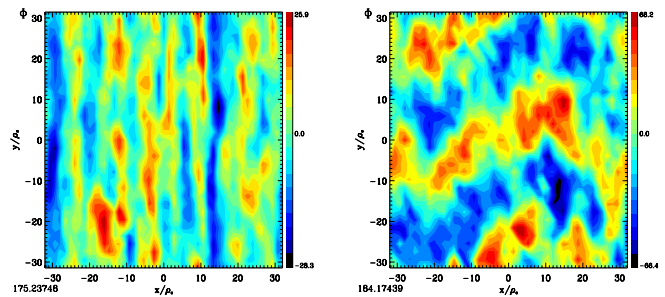


FIG. 8 (color online). Snapshots of the electrostatic potential fluctuations. Left: The baseline case indicates strong ZF activity. Right: The case with zeroed out ZFs reveals a population of distorted streamerlike structures.

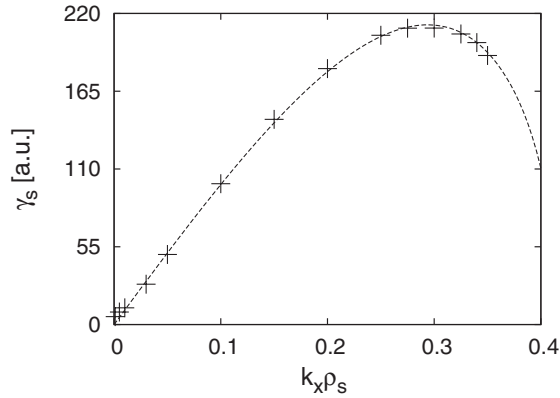


FIG. 9.  $k_x$  spectrum (for  $k_y \rho_s = 0.2$ ) of the Rogers-type secondary instability for the W7-X stellarator. This curve is in quite good agreement with that predicted from a Hasegawa-Mima analysis.

have a growth rate which is proportional to the amplitude of the driving mode. One expects that saturation is reached for a given (long-wavelength) ITG mode when its linear growth rate  $\gamma$  is balanced by the (maximum) growth rate  $\gamma_s$  of the secondary. In Ref. [15], a semianalytical investigation of secondary instabilities has been carried out, employing simple Hasegawa-Mima-type fluid models, and a generalization to three-dimensional gyrokinetics and tokamak geometry has been discussed in Ref. [16]. Following the approach outlined in Ref. [16], i.e., freezing an ITG streamer at large amplitude and considering the response of all modes constituting a secondary, one gets the result shown in Fig. 9 (this may be compared with Fig. 4 in Ref. [15]). An inspection of the parallel mode structure of the secondary identifies it as a Rogers-type mode in the sense of Ref. [16], i.e., it is driven by perpendicular (not parallel) flow shear. Comparing the value of  $\gamma_s$ —maximized over  $k_x$  and evaluated at  $\phi = \phi_{\text{sat}}$ —with that of the respective  $\gamma$  at low  $k_y$ , one finds that they are in rough balance (up to a factor of less than 2). Together with Fig. 8 (right-hand side) which can be interpreted as a streamer becoming unstable to a Kelvin-Helmholtz-like secondary, this is strong evidence for the validity of the secondary instability scenario described above. It sets an upper limit for the ion heat flux caused by adiabatic ITG modes in the W7-X stellarator, which is still moderate.

Finally, we would like to make a few comments on the nonlinear generation and saturation of zonal flows in the regular simulations. In tokamaks, zonal flow creation is usually attributed to modulational instabilities which are known to be closely connected to secondary instabilities (see Ref. [17] and references therein). Three-wave parametric instabilities are generally ruled out on the basis of a frequency mismatch argument [13]. We have found, however, that the latter does not apply in the present case because the mode frequencies (real and imaginary parts) do not change significantly with  $k_x$  for  $k_x \lesssim k_y$ . This opens

the window for a competition between parametric and modulational instabilities. Moreover, we found in nonlinear GENE simulations that collisional damping of zonal flows [18] is quite ineffective. For instance, adding ion-ion collisions with  $\nu_{ii} R/c_s = 0.05$  using a Lorentz collision operator, the changes of the transport level are less than 10% for  $R/L_{T_i} = 18$ . Thus, collisions cannot be used to boost the turbulent heat flux significantly.

In summary, we have shown and discussed results from the first nonlinear gyrokinetic simulations of ITG turbulence (using adiabatic electrons and leaving the nonadiabatic case for future work) for an optimized stellarator, namely the W7-X stellarator. Despite several similarities of the turbulence characteristics with those in a typical axisymmetric configuration, there are also very significant differences. These include comparatively moderate transport levels, a different flux-gradient relationship, the coexistence of ion-temperature-gradient modes with trapped ion modes in the saturated turbulent state, as well as the generation of zonal flows. Our results show that the three-dimensional nature of the stellarator fields may be used to affect and optimize not only the neoclassical (collisional) transport, but also the anomalous (turbulent) one.

We would like to thank T. Dannert and T. Hauff for useful discussions. The computations were performed at the Garching Computing Center. In addition, one of the authors (P.X.) gratefully acknowledges funding from a Marie-Curie contract.

- 
- [1] J. Nührenberg and R. Zille, Phys. Lett. A **114**, 129 (1986).
  - [2] W. Horton, D. I. Choi, and W. M. Tang, Phys. Fluids **24**, 1077 (1981).
  - [3] E. A. Frieman and L. Chen, Phys. Fluids **25**, 502 (1982).
  - [4] F. Jenko and A. Kendl, New J. Phys. **4**, 35 (2002); Phys. Plasmas **9**, 4103 (2002).
  - [5] L. Villard *et al.*, Nucl. Fusion **44**, 172 (2004).
  - [6] G. Rewoldt, L.-P. Ku, and W. M. Tang, Phys. Plasmas **12**, 102512 (2005).
  - [7] P. Xanthopoulos and F. Jenko, Phys. Plasmas **14**, 042501 (2007).
  - [8] X. Bonnin *et al.*, Nucl. Fusion **45**, 22 (2005).
  - [9] F. Jenko *et al.*, Phys. Plasmas **7**, 1904 (2000).
  - [10] T. Dannert and F. Jenko, Phys. Plasmas **12**, 072309 (2005).
  - [11] P. Xanthopoulos and F. Jenko, Phys. Plasmas **13**, 092301 (2006).
  - [12] A. M. Dimits *et al.*, Phys. Plasmas **7**, 969 (2000).
  - [13] P. H. Diamond *et al.*, Plasma Phys. Controlled Fusion **47**, R35 (2005).
  - [14] T. S. Hahm *et al.*, Phys. Plasmas **6**, 922 (1999).
  - [15] W. Dorland *et al.*, Phys. Rev. Lett. **85**, 5579 (2000).
  - [16] F. Jenko and W. Dorland, Phys. Rev. Lett. **89**, 225001 (2002).
  - [17] D. Strintzi and F. Jenko, Phys. Plasmas **14**, 042305 (2007).
  - [18] Z. Lin *et al.*, Phys. Rev. Lett. **83**, 3645 (1999).